

Inelastic neutron scattering peak in Zn substituted $\text{YBa}_2\text{Cu}_3\text{O}_7$

N. Bulut

Department of Mathematics, Koç University, Istinye, 80860 Istanbul, Turkey
(April 6, 2018)

The effects of nonmagnetic impurities on the neutron scattering intensity are studied for a model of the copper oxide layers in the normal state. The contribution to the $\mathbf{Q} = (\pi, \pi)$ neutron scattering intensity from processes involving the scattering of the spin-fluctuations from an impurity with large momentum transfers are calculated within the random phase approximation. It is shown that this type of scatterings could lead to a peak in the neutron scattering intensity in the normal state.

PACS Numbers: 74.62.Dh, 74.72.Bk, 75.10.Lp, 74.25.-q

An important feature found by the neutron scattering experiments on $\text{YBa}_2\text{Cu}_3\text{O}_7$ is a resonant peak which is observed at 41 meV energy and $\mathbf{Q} = (\pi, \pi)$ momentum transfers [1–3]. In this material, the peak is observed only in the superconducting state. The theories which have been put forward attribute the resonant peak to an instability in the particle-particle [4,5] or the magnetic channels [6–8]. It is of interest to determine how much each of these two channels contribute to the resonant peak in $\text{YBa}_2\text{Cu}_3\text{O}_7$.

Nonmagnetic Zn impurities have been used as a probe of the magnetic correlations in NMR experiments, and yielded valuable information [9]. Neutron scattering experiments on Zn substituted $\text{YBa}_2\text{Cu}_3\text{O}_7$ also find that the Zn impurities have important effects on the spin fluctuation spectrum [10,11]. Upon substituting 0.5% Zn, the resonant peak of the superconducting state becomes observable in the normal state as a broadened peak centered at 40 meV with a width of 10 meV [11]. As the temperature is lowered, the peak intensity increases smoothly without any observable discontinuity in the slope at the superconducting transition at $T_c = 87^\circ\text{K}$. It is found that significant amount of spectral weight develops in the peak already in the normal state. For instance, at 94°K the amplitude of the neutron scattering intensity is about half of its value at 22°K . In this sample, there is no observable spectral weight at frequencies less than ~ 35 meV. However, when the concentration of the impurities is increased to 2%, the neutron scattering intensity develops weight at frequencies as low as 5 meV, and a broad peak is observed at about 35 meV [10]. The momentum width of the structure at 35 meV is about 0.5 \AA^{-1} , which is twice that of the peak in the sample with 0.5% Zn. These are the main features of the changes induced by the Zn impurities. Understanding the reason for why dilute Zn impurities induce a peak in the neutron scattering intensity in the normal state would be useful for understanding the origin of the resonant peak in pure $\text{YBa}_2\text{Cu}_3\text{O}_7$ [11].

Here, the effects of dilute Zn impurities on the neutron scattering spectral weight $\text{Im } \chi(\mathbf{Q}, \omega)$ will be studied for a two-dimensional model of the layered cuprates in the normal state. The contributions to $\text{Im } \chi(\mathbf{Q} = (\pi, \pi), \omega)$

from processes involving the scattering of the spin fluctuations from an impurity with large momentum transfers near $2\mathbf{k}_F$, where \mathbf{k}_F is the Fermi momentum, are calculated within the random phase approximation (RPA). It will be seen that this type of scatterings could lead to a peak in $\text{Im } \chi(\mathbf{Q} = (\pi, \pi), \omega)$ in the normal state at $\omega_0 = 2|\mu|$, where μ is the chemical potential.

During the scattering of the spin fluctuations from an impurity, momentum is not conserved and, hence, the $\mathbf{Q} = (\pi, \pi)$ component of the spin fluctuations could get mixed with the other wave vector components. For instance, if momentum \mathbf{Q}^* is transferred during a scattering, then the $\mathbf{Q} = (\pi, \pi)$ component of the spin fluctuations would get mixed with the $\mathbf{q} = \mathbf{Q} - \mathbf{Q}^*$ component. This process could be considered as an umklapp scattering of the spin fluctuations by the impurity potential. It has been previously noted that this type of scatterings with large momentum transfers could play a role in enhancing the uniform susceptibility as antiferromagnetic correlations develop in Zn substituted $\text{YBa}_2\text{Cu}_3\text{O}_{7-\delta}$ [12]. It has been also shown that without the umklapp scatterings, the main effect of the impurities on $\text{Im } \chi(\mathbf{Q}, \omega)$ is to cause a smooth smearing [13]. Here, it will be shown that, when included within RPA, the scattering of the spin fluctuations with momentum transfers $\mathbf{Q}^* \approx 2\mathbf{k}_F$ can lead to a peak in $\text{Im } \chi(\mathbf{Q}, \omega)$ near ω_0 in the normal state. The underlying reason for this is that there is a kinematic constraint against creating a particle-hole pair with center-of-mass momentum $\mathbf{q} = (\pi, \pi) - 2\mathbf{k}_F$ and energy $\omega > \omega_0$. On the other hand, the scattering of the spin fluctuations with momentum transfers away from $2\mathbf{k}_F$ has a smaller effect on $\text{Im } \chi(\mathbf{Q}, \omega \approx \omega_0)$.

In the following, the two-dimensional Hubbard model will be used to model the magnetic correlations of the pure system, and a static potential will be used to model the effective interaction between the electrons and a nonmagnetic impurity. The two-dimensional single-band Hubbard model is defined by

$$H = -t \sum_{\langle ij \rangle, \sigma} (c_{i\sigma}^\dagger c_{j\sigma} + c_{j\sigma}^\dagger c_{i\sigma}) + U \sum_i c_{i\uparrow}^\dagger c_{i\uparrow} c_{i\downarrow}^\dagger c_{i\downarrow} - \mu \sum_{i, \sigma} c_{i\sigma}^\dagger c_{i\sigma}, \quad (1)$$

where $c_{i\sigma}$ ($c_{i\sigma}^\dagger$) annihilates (creates) an electron with spin σ at site i , t is the near-neighbor hopping matrix element and U is the onsite Coulomb repulsion. For simplicity, the hopping t , the lattice constant a and \hbar are set to 1.

When an impurity is introduced at site \mathbf{r}_0 of the system described by Eq. (1), the translational invariance is broken and, in this case, the magnetic susceptibility is defined as

$$\chi(\mathbf{q}, \mathbf{q}', i\omega_m) = \int_0^\beta d\tau e^{i\omega_m\tau} \langle m^-(\mathbf{q}, \tau) m^+(\mathbf{q}', 0) \rangle, \quad (2)$$

where $m^+(\mathbf{q}) = N^{-1/2} \sum_{\mathbf{p}} c_{\mathbf{p}+\mathbf{q}\uparrow}^\dagger c_{\mathbf{p}\downarrow}$, $m^-(\mathbf{q}) = (m^+(\mathbf{q}))^\dagger$, and $\omega_m = 2m\pi T$. The susceptibility defined by Eq. (2) has both diagonal $\mathbf{q} = \mathbf{q}'$ and off-diagonal $\mathbf{q} \neq \mathbf{q}'$ terms. If a static effective interaction is assumed between the impurity at site \mathbf{r}_0 and the electrons, then the RPA expression for χ in the Hubbard model becomes

$$\chi(\mathbf{q}, \mathbf{q}', i\omega_m) = \chi_0(\mathbf{q}, \mathbf{q}', i\omega_m) + U \sum_{\mathbf{q}''} \chi_0(\mathbf{q}, \mathbf{q}'', i\omega_m) \chi(\mathbf{q}'', \mathbf{q}', i\omega_m), \quad (3)$$

where $\chi_0(\mathbf{q}, \mathbf{q}', i\omega_m)$ is the irreducible susceptibility dressed with the impurity scatterings, but not with the Coulomb correlations. Here, the diagonal $\mathbf{q} = \mathbf{q}'$ terms of the irreducible susceptibility $\chi_0(\mathbf{q}, \mathbf{q}', i\omega_m)$ will be approximated by the Lindhard function of the pure system, $\chi_0^L(\mathbf{q}, i\omega_m)$. This is a good approximation since it is already known from previous calculations that the effect of impurity scattering on the diagonal irreducible susceptibility is to cause a smooth suppression [13], and this has a small effect compared to the nearly singular contribution arising from the umklapp processes. The $\mathbf{q} \neq \mathbf{q}'$ off-diagonal terms of $\chi_0(\mathbf{q}, \mathbf{q}', i\omega_m)$ will be calculated in the lowest order in the strength of the effective electron-impurity interaction as shown diagrammatically in Fig. 1(a). It will be seen that, within this model, the impurity induced changes in the $\mathbf{Q} = (\pi, \pi)$ spin-fluctuation spectrum are closely related to the spectrum of the irreducible off-diagonal susceptibility $\chi_0(\mathbf{Q}, \mathbf{q}, \omega)$ with $\mathbf{q} = \mathbf{Q} - 2\mathbf{k}_F$. After including the effects of the impurity scatterings and the Coulomb correlations, the impurity averaging is done by averaging over the impurity location \mathbf{r}_0 , which sets $\mathbf{q} = \mathbf{q}'$. This way, one obtains $\chi(\mathbf{Q}, \mathbf{Q}, i\omega_m)$, which gives the neutron scattering spectral weight after analytic continuation $i\omega_m \rightarrow \omega + i\delta$. In the following, $\chi(\mathbf{Q}, \mathbf{Q}, i\omega_m)$ will be denoted by $\chi(\mathbf{Q}, i\omega_m)$.

A static effective electron-impurity interaction for an impurity located at site \mathbf{r}_0 can be written as

$$V_{eff} = \frac{1}{N} \sum_{\mathbf{k}} e^{i\mathbf{k}\cdot\mathbf{r}_0} V_{\mathbf{k}} \sum_{\mathbf{p}, \sigma} c_{\mathbf{p}+\mathbf{k}\sigma}^\dagger c_{\mathbf{p}\sigma}, \quad (4)$$

which involves scatterings with all possible wave vectors. It has been noted that the electronic correlations play a role in determining the structure of $V_{\mathbf{k}}$ [14]. It will be seen that for $\omega \approx \omega_0$ the important scatterings are the

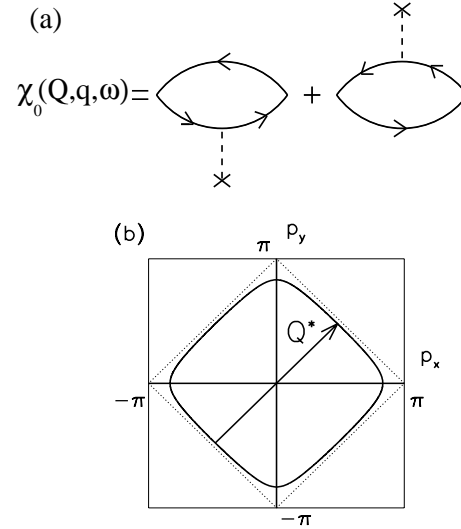


FIG. 1. (a) Feynman diagrams representing the lowest order terms of the irreducible umklapp susceptibility $\chi_0(\mathbf{Q}, \mathbf{q}, \omega)$. (b) Sketch of a single-particle scattering process involving $\mathbf{Q}^* = 2\mathbf{k}_F$ momentum transfer in the Brillouin zone. Here \mathbf{k}_F is the Fermi wave vector along (1,1) and the solid curve represents the Fermi surface of the noninteracting system at finite hole doping.

ones which transfer $\mathbf{Q}^* = 2\mathbf{k}_F$, since in this case $\chi_0(\mathbf{Q}, \mathbf{q}, \omega)$ with $\mathbf{q} = \mathbf{Q} - \mathbf{Q}^*$ has nearly singular behaviour. For other values of \mathbf{Q}^* , $\chi_0(\mathbf{Q}, \mathbf{q}, \omega)$ is a smooth function of ω with small amplitude. Hence, Eq. (3) will be solved by using only the \mathbf{Q}^* component of Eq. (4),

$$V_0 \sum_{\mathbf{p}, \sigma} c_{\mathbf{p}+\mathbf{Q}^*\sigma}^\dagger c_{\mathbf{p}\sigma}, \quad (5)$$

where $V_0 = V_{\mathbf{Q}^*}$ is taken as a parameter. Since the important umklapp contributions originate from a small range of values of \mathbf{Q}^* near $2\mathbf{k}_F$, this is a reasonable approximation. This procedure for solving Eq. (3) was necessary, because the calculation needs to be carried out on a large lattice in order to have sufficient frequency resolution. A single-particle scattering process given by Eq. (5) is illustrated in Fig. 1(b) for $\mathbf{Q}^* = 2\mathbf{k}_F$ momentum transfer in the Brillouin zone.

Within the presence of the scattering term given by Eq. (5), the solution of the RPA expression, Eq. (3), becomes

$$\chi(\mathbf{Q}, \omega) = D^{-1} \left\{ \chi_0^L(\mathbf{Q}, \omega) (1 - U\chi_0^L(\mathbf{q}, \omega)) + 4U(\chi_0(\mathbf{Q}, \mathbf{q}, \omega))^2 \right\}, \quad (6)$$

where $D = (1 - U\chi_0^L(\mathbf{Q}, \omega))(1 - U\chi_0^L(\mathbf{q}, \omega)) - 4(U\chi_0(\mathbf{Q}, \mathbf{q}, \omega))^2$ and $\mathbf{q} = \mathbf{Q} - \mathbf{Q}^*$. Here, the factor of 4 multiplying $(\chi_0(\mathbf{Q}, \mathbf{q}, \omega))^2$ is to take into account the scatterings with momentum transfers $(\pm Q^*, \pm Q^*)$ and $(\pm Q^*, \mp Q^*)$, where $\mathbf{Q}^* = (Q^*, Q^*)$. The expression

for the irreducible umklapp susceptibility $\chi_0(\mathbf{Q}, \mathbf{q}, i\omega_m)$, which is illustrated in Fig. 1(a), is given by

$$\chi_0(\mathbf{Q}, \mathbf{q}, i\omega_m) = -V_0 \frac{T}{N} \sum_{\mathbf{p}, i\omega_n} \left\{ G_0(\mathbf{p} + \mathbf{Q}, i\omega_n + i\omega_m) \right. \\ \times G_0(\mathbf{p}, i\omega_n) G_0(\mathbf{p} + \mathbf{Q} - \mathbf{q}, i\omega_n) \\ \left. + G_0(\mathbf{p}, i\omega_n) G_0(\mathbf{p} + \mathbf{q}, i\omega_n + i\omega_m) \right. \\ \left. \times G_0(\mathbf{p} + \mathbf{Q}, i\omega_n + i\omega_m) \right\}. \quad (7)$$

Here, $G_0(\mathbf{p}, i\omega_n) = (i\omega_n - \varepsilon_{\mathbf{p}})^{-1}$ with $\omega_n = (2n + 1)\pi T$ and $\varepsilon_{\mathbf{p}} = -2t(\cos p_x + \cos p_y) - \mu$ is the single-particle Green's function of the pure system. After summing over $i\omega_n$ in Eq. (7) analytically, the resulting sum over \mathbf{p} is carried out numerically. The Lindhard susceptibility χ_0^L used in Eq. (6) is given by

$$\chi_0^L(\mathbf{k}, \omega) = \frac{1}{N} \sum_{\mathbf{p}} \frac{f(\varepsilon_{\mathbf{p}+\mathbf{k}}) - f(\varepsilon_{\mathbf{p}})}{\omega - (\varepsilon_{\mathbf{p}+\mathbf{k}} - \varepsilon_{\mathbf{p}}) + i\delta}, \quad (8)$$

which is also evaluated numerically. The replacement of the diagonal irreducible susceptibility by the Lindhard susceptibility in solving Eq. (3) does not affect the results presented here. It has been shown in Ref. [13] that scatterings from an onsite impurity potential lead to a smooth smearing of the structure in the diagonal irreducible susceptibility. A similar effect was found for the $\omega = 0$ case in Ref. [12] using an extended impurity potential.

The following results have been obtained by using $U = 1.7$, temperature $T = 0.05$ and filling $\langle n \rangle = 0.86$. For these values of T and $\langle n \rangle$, one has $\omega_0 = 2|\mu| \approx 0.55$. Figure 2 shows results obtained for momentum transfer $\mathbf{Q}^* = 2\mathbf{k}_F$, where \mathbf{k}_F was taken along (1,1) for simplicity. In Fig. 2(a), the real and the imaginary parts of $\chi_0(\mathbf{Q}, \mathbf{q}, \omega)$ are shown. For comparison, in Fig. 2(b), the ω dependence of the Lindhard susceptibility $\chi_0^L(\mathbf{Q}, \omega)$ is shown. The solid line in Fig. 2(c) represents $\text{Im} \chi(\mathbf{Q}, \omega)$ for $V_0 = 0.05$. Also shown in this figure by the dashed line is the result for $V_0 = 0$, which corresponds to the pure case. Here, it is seen that $\text{Im} \chi_0(\mathbf{Q}, \mathbf{q}, \omega)$ is finite for $\omega < \omega_0$ with a sharp cut-off at ω_0 . The cut-off in $\text{Im} \chi_0(\mathbf{Q}, \mathbf{q}, \omega)$ is due to the fact that there is a kinematic constraint against creating a particle-hole pair with the center-of-mass momentum $\mathbf{q} = (\pi, \pi) - 2\mathbf{k}_F$ and energy $\omega > \omega_0$. In the corresponding real part there is a sharp peak at ω_0 . Both the real and the imaginary parts of $\chi_0(\mathbf{Q}, \mathbf{q}, \omega)$ play a role in suppressing the denominator of the expression in Eq. (6), and in leading to the peak in $\text{Im} \chi(\mathbf{Q}, \omega)$ at ω_0 . In this model, the peak is originating from the magnetic channel, since it is due to an instability of Eq. (3).

The spectrum of $\chi_0(\mathbf{Q}, \mathbf{q}, \omega)$ seen in Fig. 2(a) is quite different than that of the Lindhard susceptibility $\chi_0^L(\mathbf{Q}, \omega)$ seen in Fig. 2(b). In the limit $T \rightarrow 0$, $\text{Im} \chi_0(\mathbf{Q}, \omega)$ develops a gap for $\omega < \omega_0$. On the other

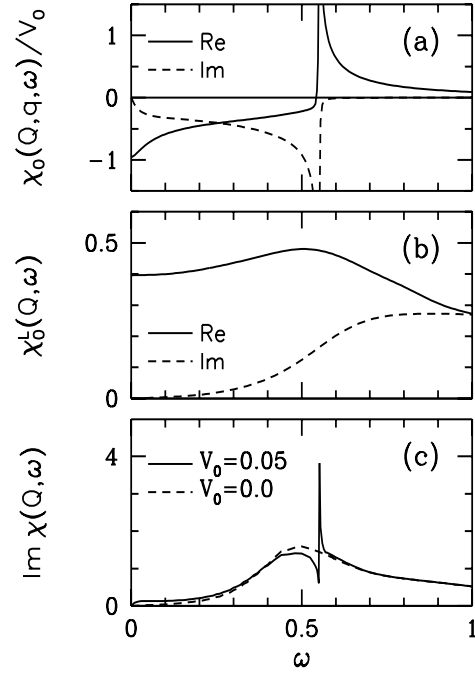


FIG. 2. (a) Irreducible umklapp susceptibility $\chi_0(\mathbf{Q}, \mathbf{q}, \omega)$ versus ω normalized by V_0 . Here $\mathbf{q} = \mathbf{Q} - \mathbf{Q}^*$. (b) Lindhard susceptibility $\chi_0^L(\mathbf{Q}, \omega)$ versus ω . (c) Spin-fluctuation spectral weight $\text{Im} \chi(\mathbf{Q}, \omega)$ versus ω for $V_0 = 0.05$ and 0.0 . These results were obtained for $\mathbf{Q}^* = 2\mathbf{k}_F$.

hand, $\text{Im} \chi_0(\mathbf{Q}, \mathbf{q}, \omega)$ is finite only for $\omega < \omega_0$. Hence, the umklapp scatterings could contribute to $\text{Im} \chi(\mathbf{Q}, \omega)$ for $\omega < \omega_0$. The quantitative features of $\text{Im} \chi(\mathbf{Q}, \omega)$ depend on the model parameters. For instance, if U is increased from 1.7 to 2.0, the hump in $\text{Im} \chi(\mathbf{Q}, \omega)$ centered at $\omega = 0.5$ grows and the dip below the peak gets smaller. The scattering of the quasiparticles by the spin fluctuations would also affect the quantitative features.

Figures 3(a) and (b) show the temperature evolution of $\chi_0(\mathbf{Q}, \mathbf{q}, \omega)$ and $\text{Im} \chi(\mathbf{Q}, \omega)$ for $V_0 = 0.05$ on a smaller ω scale. As T increases, the peak in $\text{Im} \chi(\mathbf{Q}, \omega)$ disappears. Figure 3(c) shows the development of the peak in $\text{Im} \chi(\mathbf{Q}, \omega)$ as V_0 is turned on at $T = 0.05$.

In order to have further information on the momentum and frequency structure of $\chi_0(\mathbf{Q}, \mathbf{q}, \omega)$, results on its real part are shown in Fig. 4. Figure 4(a) shows $\text{Re} \chi_0(\mathbf{Q}, \mathbf{q}, \omega)$ versus ω obtained at values of \mathbf{Q}^* which are slightly different than $2\mathbf{k}_F$, but still along (1,1). Here, the numbers next to the curves indicate the magnitude of \mathbf{Q}^* in units of $2k_F$. As \mathbf{Q}^* is varied away from $2\mathbf{k}_F$, the resonance frequency shifts and the amplitude of $\text{Re} \chi_0(\mathbf{Q}, \mathbf{q}, \omega)$ decreases. Hence, when all the contributions from scatterings with momentum transfers near $2\mathbf{k}_F$ are taken into account, one expects the peak in $\text{Im} \chi(\mathbf{Q}, \omega)$ at ω_0 to have a finite width. However, it is not possible to estimate the total spectral weight in the peak. For instance, the detailed \mathbf{k} dependence of $V_{\mathbf{k}}$ for $\mathbf{k} \sim 2\mathbf{k}_F$ is not known.

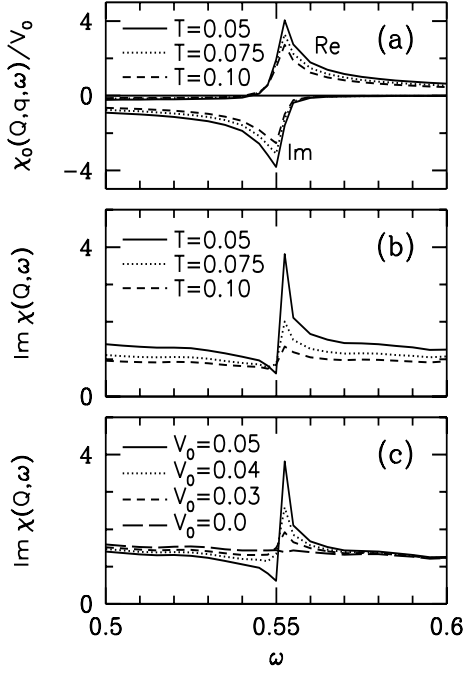


FIG. 3. Temperature variation of (a) $\chi_0(\mathbf{Q}, \mathbf{q}, \omega)/V_0$ and (b) $\text{Im } \chi(\mathbf{Q}, \omega)$ versus ω for $V_0 = 0.05$. In these two figures, the chemical potential has been kept fixed, while increasing the temperature. (c) $\text{Im } \chi(\mathbf{Q}, \omega)$ versus ω for various values of V_0 at $T = 0.05$. These results were obtained for $\mathbf{Q}^* = 2\mathbf{k}_F$.

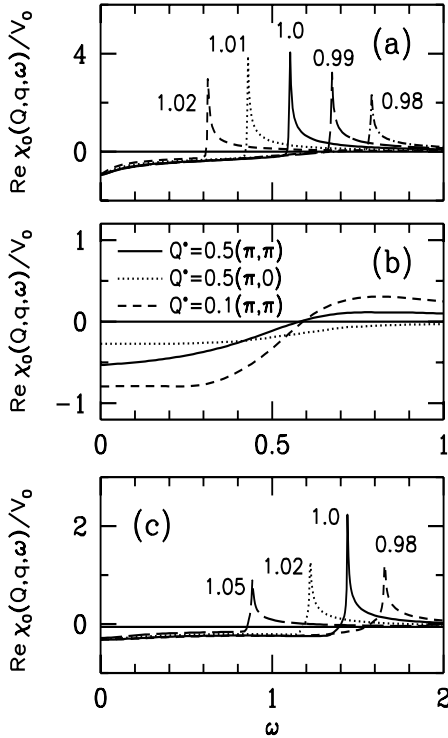


FIG. 4. $\text{Re } \chi_0(\mathbf{Q}, \mathbf{q}, \omega)/V_0$ versus ω (a) for \mathbf{Q}^* near $2\mathbf{k}_F$ and (b) for various values of \mathbf{Q}^* away from $2\mathbf{k}_F$ at $\langle n \rangle = 0.86$. (c) $\text{Re } \chi_0(\mathbf{Q}, \mathbf{q}, \omega)/V_0$ versus ω for \mathbf{Q}^* near $2\mathbf{k}_F$ at $\langle n \rangle = 0.7$.

In Fig. 4(b), $\text{Re } \chi_0(\mathbf{Q}, \mathbf{q}, \omega)$ is shown for various values of \mathbf{Q}^* away from $2\mathbf{k}_F$. Here one observes that $\text{Re } \chi_0(\mathbf{Q}, \mathbf{q}, \omega)$ is a smooth function of ω and has a much smaller amplitude near ω_0 than in the case for $\mathbf{Q}^* \approx 2\mathbf{k}_F$. Other values for \mathbf{Q}^* away from $2\mathbf{k}_F$ were also tried, but results similar to those in Fig. 4(b) were obtained. This supports keeping only the $\mathbf{Q}^* \approx 2\mathbf{k}_F$ component, Eq. (5), of the effective impurity interaction, Eq. (4), in solving the RPA equation for $\chi(\mathbf{Q}, \omega)$ at ω near ω_0 . Finally, Fig. 4(c) shows $\text{Re } \chi_0(\mathbf{Q}, \mathbf{q}, \omega)$ versus ω for \mathbf{Q}^* near $2\mathbf{k}_F$ at filling $\langle n \rangle = 0.7$, where the corresponding ω_0 is 1.44. Comparing with the results shown in Fig. 4(a), one observes that the qualitative features do not change with the band filling.

The neutron scattering experiments by Fong *et al.* [11] have found that, as the temperature is lowered below 250°K, a peak develops at $\omega = 40$ meV in $\text{Im } \chi(\mathbf{Q}, \omega)$ of 0.5% Zn substituted $\text{YBa}_2\text{Cu}_3\text{O}_7$. Here, the effects of dilute nonmagnetic impurities on $\text{Im } \chi(\mathbf{Q}, \omega)$ have been studied within a two-dimensional model in the normal state. It has been found that the impurity induced changes in $\text{Im } \chi(\mathbf{Q}, \omega)$ are closely related to the spectrum of the irreducible off-diagonal susceptibility $\chi_0(\mathbf{Q}, \mathbf{q}, \omega)$. The possibility of the structure in $\chi_0(\mathbf{Q}, \mathbf{q}, \omega)$ at $\omega \approx \omega_0$ leading to a peak in $\text{Im } \chi(\mathbf{Q}, \omega)$ has been pointed out. Within this model, the peak is due to the impurity scattering of the spin fluctuations with momentum transfers near $2\mathbf{k}_F$. However, in obtaining these results the Coulomb correlations were treated within the random phase approximation, and only the lowest order terms of $\chi_0(\mathbf{Q}, \mathbf{q}, \omega)$ have been included. It remains to be seen by how much the higher order corrections will modify the results discussed here.

The author thanks P. Bourges, H.F. Fong and B. Keimer for helpful discussions. The numerical computations reported in this paper were performed at the Center for Information Technology at Koç University.

-
- [1] J. Rossat-Mignod *et al.*, *Physica* **185-189C**, 86 (1991).
 - [2] H.A. Mook *et al.*, *Phys. Rev. Lett.* **70**, 3490 (1993).
 - [3] H.F. Fong *et al.*, *Phys. Rev. Lett.* **75** 316 (1995).
 - [4] E. Demler *et al.*, *Phys. Rev. Lett.* **75**, 4126 (1995).
 - [5] E. Demler *et al.*, *Phys. Rev. B* **58**, 5719 (1998).
 - [6] D.Z. Liu *et al.*, *Phys. Rev. Lett.* **75**, 4130 (1995).
 - [7] I.I. Mazin *et al.*, *Phys. Rev. Lett.* **75**, 4134 (1995).
 - [8] N. Bulut *et al.*, *Phys. Rev. B* **53**, 5149 (1996).
 - [9] A.V. Mahajan *et al.*, *Phys. Rev. Lett.* **72**, 3100 (1994).
 - [10] Y. Sidis *et al.*, *Phys. Rev. B* **53**, 6811 (1996).
 - [11] H.F. Fong *et al.*, *Phys. Rev. Lett.* **82**, 1939 (1999).
 - [12] N. Bulut, preprint, cond-mat/9906185.
 - [13] J.-X. Li *et al.*, *Phys. Rev. B* **58**, 2895 (1998).
 - [14] W. Ziegler *et al.*, *Phys. Rev. B* **53**, 8704 (1996).